Development of a Low Field Overhauser-Enhanced Magnetic Resonance Imaging System

Master's Thesis

Sandro Erni[1]

Advisors:

Prof. Charles M. Marcus
Harvard University

Prof. Dominik M. Zumbühl
University of Basel

June 12, 2009

[1]Sandro.Erni@stud.unibas.ch

Abstract

High image contrast in magnetic resonance imaging (MRI) can be achieved by hyperpolarizing the nuclei of interest. Dynamic nuclear polarization (DNP) is a method to create hyperpolarization where excited electron spins induce a larger nuclear spin polarization. Imaging material that has been hyperpolarized by DNP is also known as Overhauser-enhanced magnetic resonance imaging (OMRI).

An imager was designed and built to perform OMRI at low magnetic fields around 20 mT. The construction of the parts and the whole setup as well as its working principle are reported. Nuclear magnetic resonance (NMR) and MRI have been performed and have proved the operational capability of the setup. DNP was implemented and enhancements of up to 50 in the NMR signal were measured. Overhauser-enhanced imaging was performed to achieve a much better image contrast in comparison to conventional MRI.

Contents

SECTION 1

Introduction

Nuclear magnetic resonance (NMR) was first described and measured in molecular beams by Isidor Rabi in 1938 [1]. Felix Bloch [2] and Edward Mills Purcell [3] refined the technique eight years later for use on liquids and solids, for which they shared the Nobel Prize in physics in 1952 [4]. The discovery of magnetic resonance imaging (MRI) [5] followed within a couple of decades of the discovery of NMR and was a major development in diagnostic non-invasive imaging. The three-dimensional distribution of nuclear spins is imaged using radio frequency (RF) radiation in the presence of a static magnetic field with superposed pulsed field gradients. Most commonly, the spin distribution of water protons in biological systems is probed to non-invasively generate an anatomical image. The concentration of water in living tissue is such that several tens of moles contribute to the signal. The very high detection sensitivity of water protons has made MRI one of the most successful and most often used tools in clinical diagnostics [6].

Image resolution and image contrast in MRI are limited by the signal that can be detected. Better signal can be achieved by higher magnetic fields: human MRI systems use fields of up to 3 T in clinic and up to 9.4 T in research, animal-imaging magnets even range up to 15 T [7]. The signal can also be enhanced by hyperpolarizing the nuclei of interest [6]. Dynamic nuclear polarization (DNP) is a method to create hyperpolarization where electron spins are excited via electron spin resonance (ESR) to induce a larger nuclear spin polarization [8]. The corresponding imaging technique is known by two alternate names, PEDRI [9] (proton-electron double resonance imaging) and OMRI (Overhauser-enhanced magnetic resonance imaging). It uses the Overhauser effect [10, 11] to polarize protons in the presence of stable free radicals to generate highly enhanced magnetic resonance images [6]. The basic OMRI technique suffers from the need for the ESR irradiation to penetrate a biological sample, so it is implemented at low fields of less than 20 mT to have the ESR frequency below 300 MHz [12].

Most *in vivo* OMRI has focused on free radicals. Some of these compounds are stable in solution and have low toxicity [12], but nevertheless, free radicals in a body are still toxic and chances to get approval for clinical applications are low. Using nanoparticles as an alternative approach has mainly taken advantage from progress in research on functionalization of surfaces, allowing targeting [13, 14], *in vivo* tracking [14], and therapeutic action [15]. Direct imaging of hyperpolarized materials with basically no background signal has been performed and showed impressive image contrast [16, 17, 18]. Interesting for *in vivo* applications are therefore e. g. fluorine and silicon, both not naturally occurring in the body. It has been shown that silicon nanoparticles can be hyperpolarized via dynamic nuclear polarization [18, 19].

The goal of the work described in this thesis was to design and build a magnetic resonance imager to work at low magnetic fields and to be capable of performing OMRI *in vivo*. The system should be flexible and capable of performing NMR on different nuclei like ^{19}F or ^{29}Si. The setup and first results are presented in this thesis.

SECTION 2

THEORY

2.1 Nuclear Magnetic Resonance

2.1.1 Nuclear Spin

All neutrons and protons are fermions and hence have the intrinsic quantum property of spin 1/2. The overall spin of a nucleus is determined by the quantum number S. If the number of both the neutron and proton is even, the overall spin of the nucleus is zero. A non-zero spin of a nucleus is always associated with a non-zero magnetic moment (μ) with the relation $\mu = \gamma S$, where γ is the gyromagnetic ratio. The magnetic moment allows the observation of NMR, i. e. the transitions between nuclear spin levels [4].

2.1.2 Spin in a Magnetic Field

For nuclei with a spin of 1/2 (e.g. ^{1}H, ^{13}C, ^{19}F or ^{29}Si) the nucleus has two possible spin states, $m = 1/2$ and $m = -1/2$, also called spin-up and spin-down, respectively. These two states are degenerate at zero magnetic field. If a magnetic field is applied, the interaction between the nuclear magnetic moment and the external magnetic field splits the energies of the two states (Fig. 1). The energy of a magnetic moment μ in a magnetic field B_0 is given by:

$$E = -\mu B_0 \tag{1}$$

Therefore, the different nuclear spin states have different energies in a non-zero magnetic field. If γ is positive, $m = 1/2$ is the lower energy state.

The energy difference between the two states is

$$\Delta E = \gamma \hbar B_0 \tag{2}$$

and results in a small polarization in the lower energy state [4].

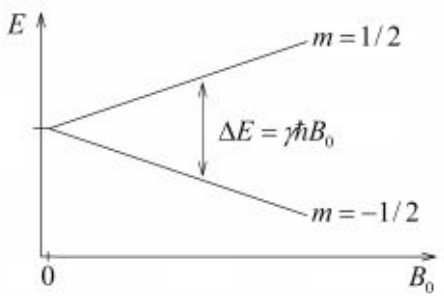

Figure 1: Splitting of nuclear spin states in a magnetic field. The energy difference between the two states is proportional to the field strength.

2.1.3 Magnetic Resonance

Nuclear spins can absorb electromagnetic radiation of the frequency matching the energy difference between the nuclear spin levels in a constant magnetic field, i. e. of the resonance frequency. The energy of an absorbed photon is then $E = \hbar\omega_0$, where ω_0 is the resonance frequency. Hence, a magnetic resonance absorption will only occur if $\Delta E = \hbar\omega_0$, which is when the resonance condition

$$\omega_0 = \gamma B_0 \tag{3}$$

is true [4].

When the magnetization has another direction than the main magnetic field, a torque is exerted on the magnetization. The torque is perpendicular to both the magnetic field and the magnetization. This results in a precession motion described by the general Bloch equation

$$\frac{d\vec{M}}{dt} = \gamma \left(\vec{M} \times \vec{B_0} \right) \tag{4}$$

in which the magnetization vector rotates around the magnetic field B_0. The angular frequency ω_0 of this precession is the same as in the resonance condition (3) [20].

2.1.4 Relaxation

The process of relaxation refers to nuclei which return to the population of a thermodynamic equilibrium in the magnetic field [4]. This process is also called T_1 or spin-lattice relaxation, where T_1 is the mean time for an individual nucleus to return to its equilibrium state. The nuclear spins can be probed again once the population is relaxed, i. e. the spins are in the initial equilibrium state.

The precessing nuclei can also fall out of alignment with each other and stop producing a signal. This transverse relaxation is also called T_2. Because of different relaxation mechanisms involved, T_1 is always longer than T_2. In a NMR measurement, the value T_2^* is basically depending on the experimental setup and the homogeneity of B_0 in particular. It is the actually observed decay time in the free induction decay (FID, the measured NMR signal). In the corresponding Fourier transform of the FID, T_2^* is inversely related to the width of the NMR signal in frequency units [21, 22].

2.1.5 Spin Polarization

Each spin placed in a magnetic field has one of the two possible states, $m = 1/2$ or $m = -1/2$. The number of spins in the lower energy level, N^-, is slightly larger than the number in the upper level, N^+. According to Boltzmann statistics the ratio is

$$\frac{N^+}{N^-} = e^{-\Delta E / k_B T} \tag{5}$$

where ΔE is the energy difference between the two spin states, k_B is Boltzmann's constant, and T is the temperature.

The ratio $\frac{N^+}{N^-}$ decreases as temperature decreases and approaches one with increasing temperature, respectively. With an increasing magnetic field and

therefore increasing ΔE, the ratio decreases and for lower fields it approaches one [22]. The spin polarization is the difference between the two populations divided by the total number of spins :

$$\frac{N^- - N^+}{N^- + N^+} \tag{6}$$

The spin polarization at room temperature and a magnetic field of 20 mT is approximately only 10^{-15}.

The signal in NMR spectroscopy results from the difference between the energy absorbed by the spins which make a transition from the lower energy state to the higher energy state, and the energy emitted by the spins which simultaneously make a transition from the higher energy state to the lower energy state. The signal is thus proportional to the spin polarization. NMR is a rather sensitive spectroscopy since it is capable of detecting these very small population differences [22].

2.2 Magnetic Resonance Imaging

2.2.1 Gradient Fields

The principle behind all magnetic resonance imaging is the resonance condition (3), which shows that the resonance frequency ω_0 of a spin is proportional to the magnetic field B_0. A gradient in the magnetic field therefore allows to relate the position of a spin to its precession frequency [23]. Normally, three specially designed coils are used to generate magnetic fields parallel to B_0 with linear gradients in one of the Cartesian directions each.

2.2.2 Slice Selection

Slice selection in MRI is the selection of spins in a plane through the object by applying the first gradient during the NMR pulse. Depending on the NMR pulse shape, only the spins in a slice of a defined thickness are affected due to the gradient in the magnetic field.

A NMR pulse of rectangular shape contains a wide range of frequencies in the Fourier space. In order to select a well defined slice, the pulse has to be narrow and well defined in the frequency space. The ideal shape therefore is a *sinc*-function

$$sinc(x) = \begin{cases} \frac{sin(x)}{x} & x \neq 0 \\ 1 & x = 0 \end{cases} \tag{7}$$

which has a square frequency distribution. An ideally shaped pulse is impossible in practice since a *sinc*-function is infinitely extended. A truncated or slightly modified *sinc*-pulse is therefore used most often [23].

2.2.3 Phase Encoding

After a slice is selected, the phase encoding gradient is turned on. It is used to impart a specific phase angle to a precessing spin depending on its location.

Considering the selected slice as a plane of precessing spins, the phase encoding gradient is applied along one of the axis of this plane. Spins along this

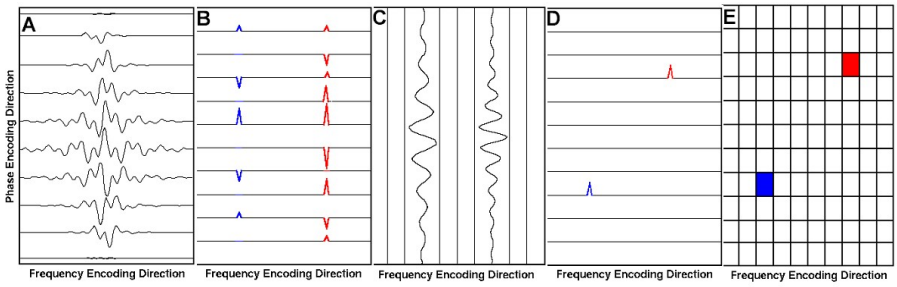

Figure 2: Example for data procession in MRI with two spins only: The acquired waveforms (A) are first Fourier transformed in the frequency encoding direction giving peaks (B) with different amplitudes where sample was detected (C). The data is then Fourier transformed in the phase encoding direction. The result are peaks only at the places where sample has been detected (D), giving a 2-dimensional image of the spin distribution (E) [23].

axis feel different magnetic fields and precess at different frequencies as long as the gradient is turned on. As soon as the gradient is turned off, all spins precess at the same frequency again but have different phases now [23].

2.2.4 Frequency Encoding

A frequency encoding gradient is turned on after phase encoding. It is perpendicular to the phase encoding gradient in the plane of the precessing spins. The principle is exactly the same as for phase encoding with the only difference that during the frequency encoding step also the readout takes place. Therefore the spins along this gradient's axis contribute signals of different frequencies to the FID depending on their position [23].

2.2.5 Data Procession

A simple Fourier transform is capable of determining the phase and frequency of the signal from a precessing spin. Unfortunately a one dimensional Fourier transform is incapable of this task when more than one spin is located within the sample at a different phase encoding position. There needs to be a step in the phase encoding gradient for each location in the phase encoding gradient direction. To resolve 64 positions along the phase encoding direction, 64 different magnitudes of the phase encoding gradient are needed and 64 different FIDs have to be recorded.

The FIDs acquired must be Fourier transformed to obtain an image of the location of spins. The signals are first Fourier transformed in the frequency encoding direction to extract the frequency domain information and then in the phase encoding direction to extract information about the position in the phase encoding gradient direction. The resulting image represents the spatial nuclear spin density distribution (Fig. 2) [23].

To reduce noise in the final image, the acquired signals can be digitally filtered with a *sine* or *sine square* filter. The FID is simply multiplied with the corresponding filter function with a maximum where most of the signal is

expected. Parts of the acquired decay where the actual signal is low are therefore attenuated.

2.2.6 Signal-to-Noise Ratio

In a magnetic resonance image, information is contained in the variation of the gray level across the image which is proportional to the signal at that position. The fundamental restriction for faster scanning and higher resolution is the signal-to-noise ratio (SNR). The signal in a pixel is due to the total magnetic moment of the spins in a voxel (3-dimensional pixel). It is proportional to the volume of the voxel considered and is therefore small for high resolution (small voxels) [20]. The random noise in a magnetic resonance imager is caused by ohmic losses in the receiving circuit which has two components: ohmic losses in the receive coil itself and eddy-current losses in the sample, which are inductively coupled to the coil [24].

A coil carrying a current I has a magnetic field $B_1(\vec{r})$ at $\vec{r}$. The coil sensitivity at that point is then $B_1(\vec{r})/I = \beta_1(\vec{r})$. The voltage S (for signal) induced by a transverse magnetization $M_T(\vec{r})$ in the coil is

$$S = \omega_0 |M_T(\vec{r})||\beta_1(\vec{r})|dV(\vec{r}) \tag{8}$$

where $dV(\vec{r})$ is the volume of the voxel considered and ω_0 is the local Larmor frequency of the resonance condition (3).

If the coil is considered as a series LCR circuit, the resistance $R = R_c + R_S$ is the sum of the coil resistance R_c and the resistance R_S induced by the sample conduction losses. The noise voltage over the resonant circuit is then

$$V_N = \sqrt{4k_B T(R_c + R_s)\delta f} \tag{9}$$

where k_B is Boltzmann's constant, T is the absolute temperature and δf is the bandwidth of the receiver. The SNR of a voxel is now found by dividing (8) by (9):

$$SNR = \frac{\omega_0 |M_T(\vec{r})||\beta_1(\vec{r})|dV(\vec{r})}{\sqrt{4k_B T(R_c + R_s)\delta f}} \tag{10}$$

Using $R_s \propto \omega_0^2 \beta_1^2$ and $R_c \propto \sqrt{\omega_0}$ leads to

$$SNR = \frac{\omega_0 |M_T(\vec{r})||\beta_1(\vec{r})|dV(\vec{r})}{\sqrt{4k_B T(A\sqrt{\omega_0} + C\omega_0^2 \beta_1^2)\delta f}} \tag{11}$$

This equation shows that at low frequencies the resistance R_c dominates, the loading by the sample can be neglected and the SNR is proportional to β_1 [20].

There has been a long dispute about the magnetic field strength dependence of the SNR [25]. The SNR depends on many different parameters like scan parameters, relaxation properties, and properties of the NMR coils. Several of these parameters also depend on the magnetic field strength [20]. Summed up, it can be stated that $SNR \propto B_0^{7/8}$ at low fields and $SNR \propto B_0$ at magnetic fields higher than 0.5 T [26].

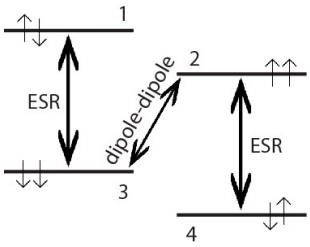

Figure 3: Energy level diagram of one electron spin (left arrow) and one nuclear spin (right arrow). ESR equalizes the populations between electron spin ground and excited states (*1* and *3*, *2* and *4*). The electron-nuclear dipole-dipole contact interaction between *2* and *3* leads to simultaneous electron and nuclear spin flips and to a nuclear polarization in state *3* and *1*.

2.3 Dynamic Nuclear Polarization

Electron spin resonance is based on the same principles as NMR but electron spins are addressed instead of nuclear spins. In a system where electron and nuclear spins are coupled through dipolar or scalar interactions, a polarization in electron spins can be transferred to some extent to the nuclear spins [9].

A free radical diluted in water is a commonly used system for DNP [27]. The free radical provides an unbound electron accessible by ESR. The polarization can be transferred to protons of a solvent in the electron's close proximity [9]. Common free radicals often used in these experiments belong to the family of nitroxide free radicals [28].

2.3.1 Overhauser Effect

The Overhauser effect for two spins 1/2 is usually described with a four-level diagram (Fig. 3) when considering only pairs of electron and nuclear spins. There are four possible energy levels labeled *1* to *4* in order of decreasing energy. At thermal equilibrium, the population of each state depends on its energy level and is given by the Boltzmann distribution (5). Level *4* has the highest population and due to much larger energies of electronic transitions relative to nuclear, the population difference between states *1* and *2* (*3* and *4*) is much smaller than that between *1* and *3* (*2* and *4*) [9].

The Overhauser effect is the perturbation of nuclear spin level populations when electron spin transitions are saturated by microwave irradiation. This irradiation equalizes populations between the ground and excited electron spin states (*1* and *3*, *2* and *4*). In a solution of free radical molecules, the predominant interaction between unpaired electron and nuclear spins is a dipole-dipole contact interaction resulting in simultaneous nuclear and electron spin flips between states *2* and *3*. The nuclear polarization ends up much greater than it would normally be. Furthermore, it actually is opposite to what is usually expected leading to a phase change of the NMR signal [6, 9]. The polarization first goes to zero and then increases to larger negative values (taking the thermal polarization as a reference). The effect is therefore called negative enhancement. Under ideal conditions and 100% saturation this would lead to an enhancement factor of -329 [29].

SECTION 3

Materials and Methods

3.1 Imager Construction

The whole setup is sitting inside a copper box to shield the environment from magnetic fields and to shield the experiment from outside electromagnetic noise. All coils have been built on differently sized acrylic tubes to fit into each other to form a layered setup (Fig. 4). The core, where the sample is placed, is sized large enough to accommodate a mouse.

The axis of the setup were defined as follows, where front means where the opening of the copper box is and with the origin at the center:

- x-axis from left to right
- y-axis from bottom to top
- z-axis from back to front

3.1.1 B_0 Magnet

A water-cooled Helmholtz electromagnet (5451 Electromagnet, GMW, San Carlos, CA) generates the main magnetic field of maximally 54 mT. It has a magnetic field of about 0.7732 mT per Ampere DC, and an inner diameter of 30 cm. The homogeneity in a sample region of a 40 mm sphere at the center was measured by the manufacturer to be less than 100 ppm (Appendix A.1).

The current in the electromagnet is controlled by a water-cooled power supply (Model 858, Danfysik, Jyllinge, Denmark) with a maximal output of 70 A. The ramp time of the power supply is relatively long, in the range of tens of seconds per Ampere. Waiting a minute for the power supply to stabilize after having set the output current is therefore essential to have a constant magnetic field over the whole duration of a measurement.

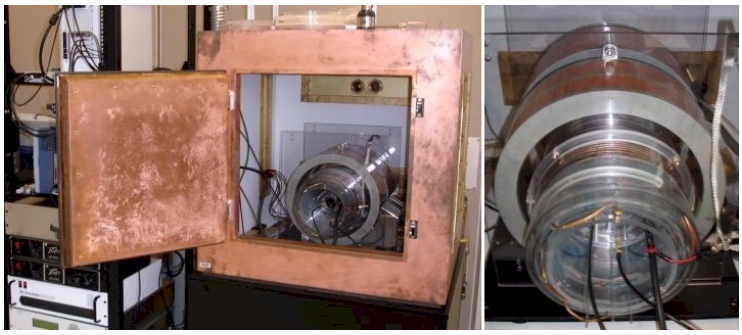

Figure 4: The setup of the whole experiment inside a shielded copper box (left) and the assembly of all coils on acrylic tubes in the Helmholtz electromagnet (right).

The current from the power supply to the magnet inside the shielded box is going through a low-pass high current filter to filter out high frequency noise on the DC line.

3.1.2 NMR Coil Design

Coils for transmitting and receiving a NMR signal need to operate at 400-1200 kHz for magnetic fields of 10-30 mT. The coils are designed as saddle coils on acrylic tubes. The tubes have an outer diameter of 5" and 2" for the transmit and receive coil, respectively. The coils are built with magnet wire, non-magnetic chip capacitors and non-magnetic tunable capacitors (Voltronics Corp., Denville, NJ) to be tunable over a certain range and to match frequencies to each other and to the magnetic field (Appendix A.2). The transmit and receive coils are oriented orthogonal to each other in the experimental setup to reduce coupling and pickup of the NMR transmit signal in the receive coil (Fig. 5).

The NMR signal generated by an arbitrary waveform generator in the control hardware (Section 3.2) is low-pass filtered (SLP-1.9, Mini-Circuits, Brooklyn, NY) and amplified with a RF power amplifier (3200L, Electronic Navigation Industries). The amplifier has a gain of 55 dB and a nominal power of 200 W. The maximal input power applied was 0 dBm.

The signal picked up in the receive coil is low-pass filtered (SLP-1.9, Mini-Circuits) and preamplified (AU-1447, Miteq, Hauppauge, NY). An RF switch (ZASWA-2-50DR, Mini-Circuits) is placed between the coil and the preamplifier to protect the latter from high voltages due to coupling to the transmit coil during the NMR pulse transmission. The preamplifier has a gain of 57 dB. The signal needs to be attenuated by 6 dB thereafter to prevent damage in the control hardware.

3.1.3 Gradient Coil Design

The coils for the gradient magnetic fields need to carry relatively high currents of up to 30 A for a short amount of time. They also need to have a very low inductance to be able to pulse with a fast ramping time. Optimized designs thereto are available [30] and have been used.

The coils have been wound with copper tubing of outer diameter 1/8". They are fixed on acrylic tubes of diameters of 7.5", 8", and 8.5", although they had to be cut afterward to fit into each other (Fig. 5). The copper tubing is used to provide better cooling to the coils. They are only air-cooled so far and don't seem to warm up significantly, but water-cooling is possible and could easily be installed if necessary.

The DC pulses from the control hardware are amplified by commercially available audio power amplifiers (CS-4000, Peavey Electronics Corporation, Meridian, MS), which have been modified to operate at low frequencies down to DC. The amplifiers are running in single channel mode at maximum power with an output of 2000 W. The output is low-pass filtered (LE100LH, Filter Concepts, Santa Ana, CA) and has a power resistor of 2 Ω (ER4-20-40T, Powerohm Resistors, Katy, TX) in series with the coils to provide the minimum load needed by the amplifier. The ramp time for the gradient coils has been set to 0.1 ms to prevent overshooting at the pulse edges due to low-pass filtering.

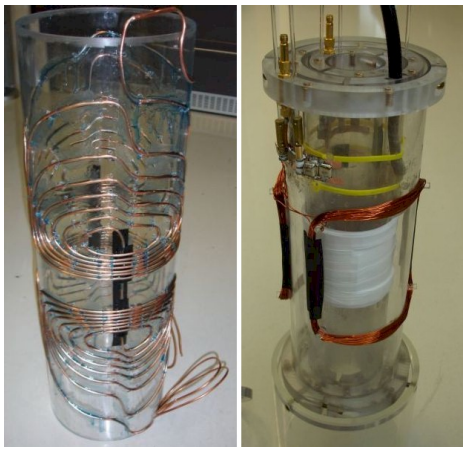

Figure 5: One gradient coil which generates a magnetic field along the tube axis with a gradient perpendicular to it (left) and the concentric assembly of NMR and ESR coils on acrylic tubes (right) with NMR transmit coil (outer), ESR transmit coil (middle), and NMR receive coil (inner).

3.1.4 ESR Coil Design

An ESR coil for in vivo applications should ideally operate at 200 - 300 MHz. The coil was designed as an Alderman-Grant resonator [31] (Appendix A.3) and built on an acrylic tube of 3.5" outer diameter to fit between the NMR transmit and receive coils. It is oriented orthogonal to the NMR receive coil to reduce noise from the ESR pulse in the acquired signal (Fig. 5). The resonator is made of 0.1 mm-thick copper sheets for the guard rings and vertical bands, and three layers of 1/32"-thick Teflon sheet as isolation between there (Fig. 6). Non-magnetic tunable capacitors (Voltronics Corp., Denville, NJ) are used to be able to tune and match the resonator.

The ESR signal from the control hardware is amplified by a RF power amplifier (BT00100-DeltaB-CW, Tomco Technologies, Norwood, Australia). The amplifier has a gain of 50 dB and a maximal output of 1 kW. The output is low-pass filtered to reduce the power of higher harmonics generated by the amplifier. The high power low-pass filter was built according to an online manual [32] with use of a program for electrical filter design (Elsie, Tonne Software) to operate at a cutoff frequency of ~ 400 MHz (Appendix A.4). The connection to the coil is made with a high power coaxial cable directly attached to the coil to reduce power loss.

3.2 Control Hardware

A PXI system (NI PXI-1044, National Instruments, Austin, TX) controls all outputs and inputs, the triggering of instruments and the timing of experimental sequences. Its components are:

- an optical fiber connection to the experiment's computer with the control software (Section 3.3),

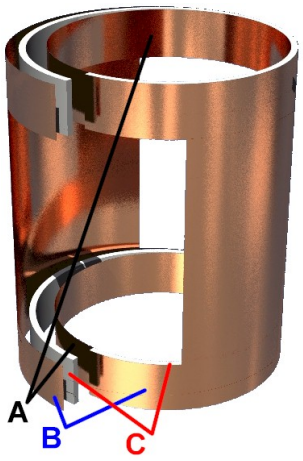

Figure 6: The ESR coil design has two guard rings (A) made of a copper sheet. One ring is connected to ground, the other one is not connected but is on ground potential due to the symmetry. The two vertical bands (B) are also made of a copper sheet. They are not connected to each other but form a capacitor with the guard rings. The Teflon (C) acts as an isolator between the guard rings and the vertical bands.

- a GPIB connection to the main magnet's power supply to set and read the output current,
- four arbitrary waveform generators to generate the NMR transmit signal and the pulses for the three gradient coils,
- a RF signal generator for the ESR signal,
- an analog-to-digital converter to read the measured NMR signal,
- and a 5 V TTL/CMOS digital output to trigger the timing of the waveform generators and to gate instruments and switches.

3.3 Control Software

All procedures to communicate with the control hardware are written in Igor Pro (WaveMetrics, Lake Oswego, OR). A user interface is implemented to control all parameters, the sequence and timing of an experiment.

3.3.1 Events Panel

The window Events Panel is the main user interface (Fig. 7). It allows designing an experiment using different channels to address different parts of the hardware and using events for the timing. The panel, all its functions and procedures including compiling a given sequence are programmed in the file `EventsPanel.ipf` and can be modified there if necessary.

At the top of the Events Panel, several overall parameters for an experiment are set:

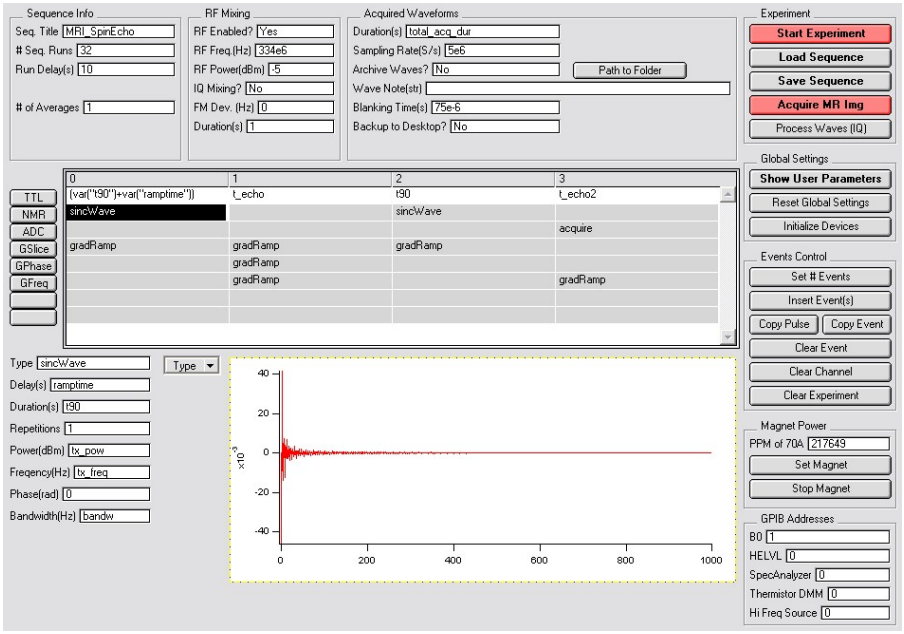

Figure 7: Events Panel showing a spin echo imaging sequence. See text for more details.

- General information about the sequence, including a name, the number of runs and averages and the delay time between two runs.
- Parameters for an ESR pulse, which will be applied before every run of an experiment if ESR is enabled. The frequency, duration and power of the pulse can be set.
- Parameters for the acquisition, including the duration, sampling rate, a general note to be attached to the acquired wave, and a time for which the switch between receive coil and digitizer is still shut (blanking time).

The column to the right contains buttons to start running an experiment or an image acquisition, to load previously saved sequences into the panel including all parameters, and also save modified sequences. Further down, buttons to clear, copy and insert events and channels help modifying a sequence. Below, the magnet current can be set as parts per million of 70 A. GPIB addresses of commonly used instruments can be set at the very bottom.

The main part of the Events Panel in the middle is a table to design the experiment's sequence where the rows stand for different channels and the columns are subsequent events. The action of every channel can be determined for each event. The events are numbered at the top, starting from 0. The total number of events can be changed by the controls to the right.

The channels are named to the left. The names stand for the parts of the PXI system to be controlled and have to be identical with the name assigned to the parts in National Instrument's Measurement & Automation software installed for the PXI:

- TTL stands for the 5 V TTL/CMOS digital output and is used in the Events Panel to set the duration of each event and to define loops over one or several events.
- NMR is the output of the NMR transmission pulse waveform generator.
- ADC stands for the analog-to-digital converter for the signal acquisition, where a name for the acquired waves can be defined and averaging can be turned on or off.
- GSlice, GPhase, and GFreq control the three gradient waveform generators.

By clicking on the button with the name on it, a new name can be assigned and type, trigger line and gate line can be changed.

By selecting a single cell in the table, a pulse can be chosen for that particular channel at this particular event from the Type list below the table. The parameters for the chosen pulse shape then can be entered. A general shape of the pulse is shown to the right. Some general waves and variables used by the experiment or the Events Panel are stored in the experiment's Igor directory `root:events`, including two text waves representing the pulse shapes and parameters for each event and channel (`eventsWave`), and the timing (`sequenceWave`).

3.3.2 User Parameters

The window User Parameters allows setting parameters that are often used. These values can be referred to from other user parameters or from the Events Panel. User parameters are saved as strings in the experiment's Igor directory `root:userParams`.

3.4 Sequence Design

The sequence used for imaging was a spin echo sequence (Fig. 8) [23]. A 90° *sinc*-shaped NMR pulse is applied for a time t_{90} while the slice selecting gradient is on. Phase and frequency encoding gradients are turned on during a time t_{echo} after the slice selecting gradient is turned off. Thereafter, the slice selecting gradient is turned on again for the echo, i. e. a 180° *sinc*-shaped NMR pulse of t_{90} (with double the power compared to the 90°-pulse). The slice selecting gradient is turned off and the frequency encoding gradient is turned on for the readout of the signal, which occurs t_{echo} after the second pulse. A new sequence with a different phase encoding gradient can be started after the repetition time t_R. t_R normally is longer than T_1 of the sample to let all spins be in equilibrium again [33]. The first lobe of the frequency encoding gradient is to compensate for dephasing of spins in the frequency encoding direction during the first part of the acquisition; the negative lobe of the slice selecting gradient is to compensate for dephasing during the 90° NMR pulse.

The *sinc*-shape used is a truncated *sinc* with at least four zero-crossings, better are six or eight zero-crossings. The more zero-crossings the *sinc*-pulse has, the better is the rectangular frequency distribution but the more time is needed for the whole pulse.

No slice selecting gradient is needed and the NMR pulses don't need to be *sinc*-shaped if a projection of the whole sample onto one plane is acquired and no slice of the sample needs to selected.

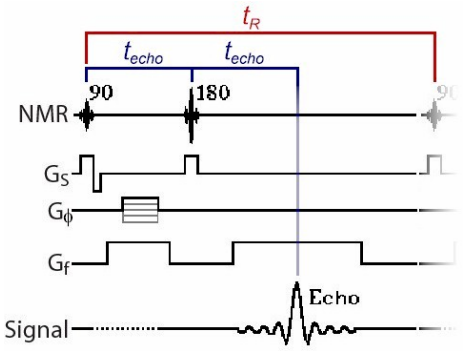

Figure 8: Spin echo sequence showing the pulses for NMR transmission, slice selecting, phase encoding, and frequency encoding gradients. The acquired signal is shown at the bottom. The phase encoding gradient is varying for each acquisition run. Echo time (t_{echo}) and repetition time (t_R) are indicated.

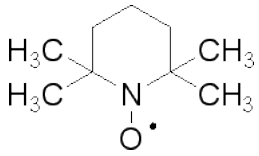

Figure 9: TEMPO free radical with an unbound electron at the oxygen.

To perform DNP experiments, simply an ESR pulse is applied before a sequence to hyperpolarize the material. The pulse is stopped right before the transmission of the NMR pulse. An ESR pulse is applied before each spin echo sequence to image hyperpolarized material.

3.5 Samples

Glass bottles with a volume of 60 ml, an outer diameter of 42 mm and an overall length of 83 mm were used as sample containers. Gadolinium doped (~ 1.5 mM) water was used for most NMR and imaging experiments. A nitroxide free radical called TEMPO (Fig. 9) (2,2,6,6-Tetramethyl-1-piperidinyloxy 98 %, Sigma-Aldrich, St. Louis, MO) was used in the DNP experiments and for hyperpolarized imaging. Mostly, 50 - 60 ml of a sample were used. Some bottles have been slightly modified for imaging purposes.

SECTION 4

Results and Discussion

4.1 Magnetic Resonance Imaging

4.1.1 NMR Experiments

NMR measurements on water samples were first taken to show the operational capability of the NMR coils and setup. Normally, a flip angle calibration was performed to find t_{90} for a specific set of coils and sample (Fig. 10).

4.1.2 Projection Imaging

Proton resonance imaging was started using a spin echo sequence to acquire projection images (Fig. 11). The acquired waveforms were digitally filtered with a sin^2 function before the 2-dimensional Fourier transform was applied. Averaging over several acquisition was needed to form an image of reasonable quality.

It was shown that magnetic resonance imaging at low fields of 18 mT works quite well. Image quality was improved a lot by adding electrical filters to the gradient coil lines. Low-pass filtering those prevents noise picked up outside to get into the setup via the gradient coils.

4.1.3 Slice-Selected Imaging

Slice selection was applied to image a cross-section of a given sample (Fig. 12). It was proved to work in the same setup, with a lot of averaging though since the signal is much weaker. By performing this step the imager was shown to be fully functional and in principle capable of acquiring 3-dimensional magnetic resonance images.

4.1.4 Gradient Fields

The magnetic field of the three gradient coils was mapped before the first images were acquired (Fig. 13). The maps were taken in xz- and yz-plane at $y = 0$ and $x = 0$, respectively, for each gradient coil. The results show that the magnetic fields are not perfectly linear and also have components in the other two directions. It was nevertheless decided that for the research to be done on the setup the fields are accurate enough.

Later on, small sample tubes have been imaged to show the consequences of the gradient distortion on an actual image (Fig. 14). These images then showed a significant distortion mainly in x- and y-direction. To prove the operational capability of the system and the concept of new ideas these gradients should nonetheless be sufficient.

4.2 Dynamic Nuclear Polarization

Water proton spins were hyperpolarized with TEMPO free radical by applying an ESR pulse before a NMR measurement. The NMR signal was enhanced by

factors up to 50 (Fig. 15). It was therefore proven that the parts for dynamic nuclear polarization are also working.

4.2.1 RF Power

Several steps had to be taken to have DNP working reasonably low RF power levels comparable to values found in literature [9].

- The ESR pulse has to be stopped right before the start of a NMR experiment. If it was stopped too early, the polarization had returned to its thermal equilibrium due to a short T_1. If it wasn't stopped until the end of the NMR experiment, the acquired NMR signal was very noisy due to cross-talk between the ESR coil and the NMR receive coil.
- The number of connectors to lead the signal to the ESR resonator was reduced by attaching a high power coaxial cable directly to the coil. The transmitted signal had been reflected partially at every connection leading to power loss and significant heating in connectors and cables.
- The output of the RF power amplifier had to be low-pass filtered because it puts out a lot of power (up to -12 dBc) at higher harmonics. This signal ended up in the tuned ESR coil as off-resonant noise which led to significant heating of the resonator itself causing a shift of the coil's resonance peaks.
- The originally measured g-factor of TEMPO free radical at high magnetic field differed by about 2.5 % from the actual g-factor in the low-field setup. The new g-factor was found by sweeping the frequency (Fig. 16), giving a significant increase of the effect of DNP.

4.2.2 Sample Heating

The ESR pulsing at frequencies around 300 MHz is also acting like a microwave because electric fields are generated simultaneously with magnetic fields. Significant heating of the water sample can therefore be observed when constantly doing DNP experiments (Fig. 17). The Alderman-Grant resonator used in the experiments is designed to reduce electric fields and therefore sample heating [31]. To avoid heating in the present setup, the power of the ESR pulse can be reduced giving less enhancement though. A compromise has to be found between magnitude of enhancement and heating amount, depending on the overall duration of an experiment and the duration of each ESR pulse.

4.3 Hyperpolarized Imaging

Imaging of hyperpolarized material is possible by combining the techniques of MRI and DNP (Figs. 18, 19). It needs less averaging and is much faster than conventional imaging due to the much stronger signal. The comparison of two images, non-hyperpolarized and hyperpolarized, shows an impressive difference and proves the significance of hyperpolarized imaging to achieve high image contrast in MRI.

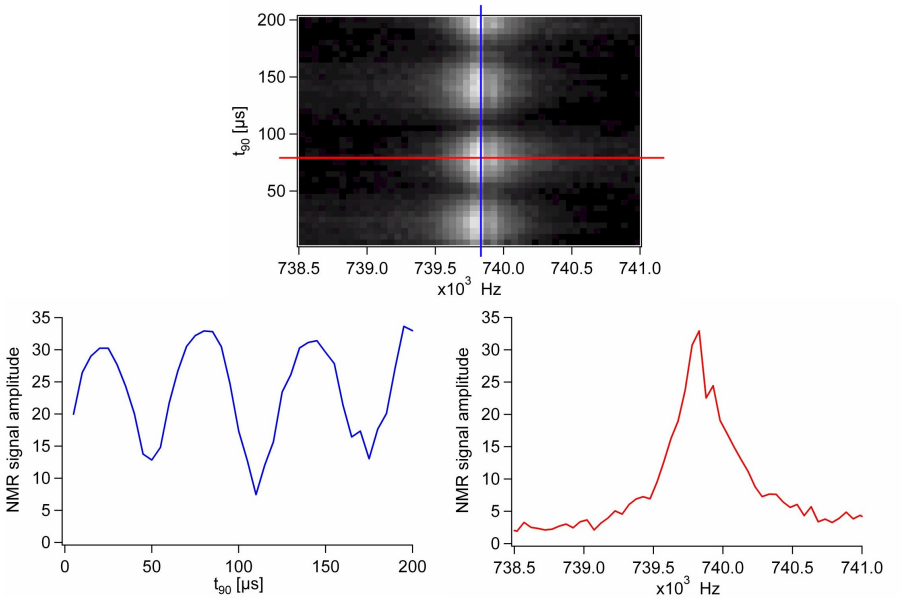

Figure 10: A 2-dimensional plot (top) with each row being a Fourier transform of an FID with a different t_{90}. A vertical cut at the signal frequency (left) shows the Rabi oscillations, i. e. the periodic dependence of the NMR signal amplitude on the duration of the NMR pulse. The correct t_{90} for a 90° flip angle can be read out to be $\sim 25\mu s$. A horizontal cut at t_{90} (right) shows the typical NMR signal peak at the frequency corresponding to B_0.

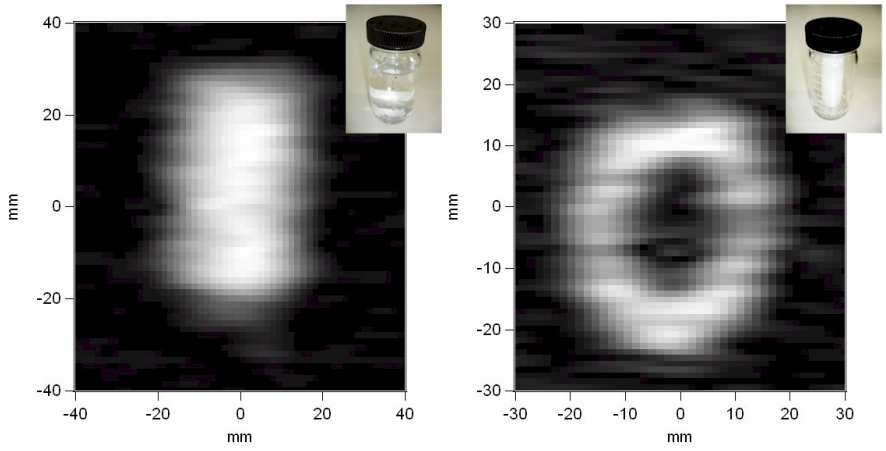

Figure 11: Projection image showing a coronal view of a bottle filled with water (left) and an axial view of a bottle with water and a plastic rod in the center (right). The insets are photographs of the actual used samples. The images are taken at a magnetic field of 18 mT with an echo time of 0.5 ms and show an average over 50 acquisitions.

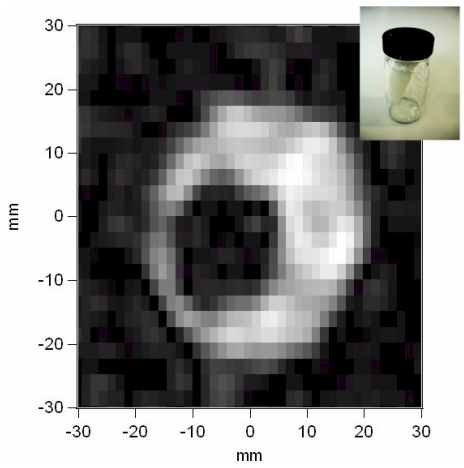

Figure 12: Slice selected image showing an axial view of a bottle with water and a tilted plastic rod inside. The inset is a picture of the sample. Slice thickness is 5 mm. The image is taken at a magnetic field of 18 mT with an echo time of 1 ms and shows an average over 1000 acquisitions.

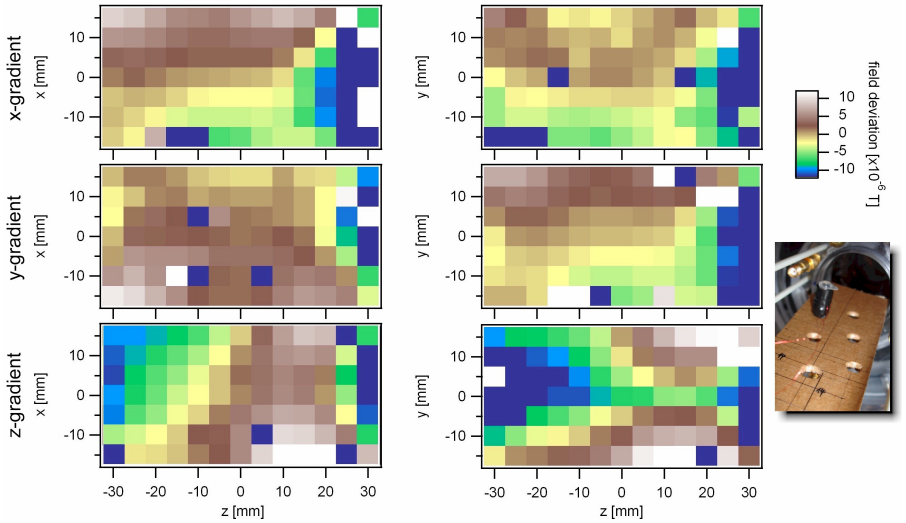

Figure 13: The magnetic fields of the gradient coils have been mapped using a small sample tube with a NMR receive coil wound around it (inset). The maps show gradients that are more or less linear with some components in the other directions.

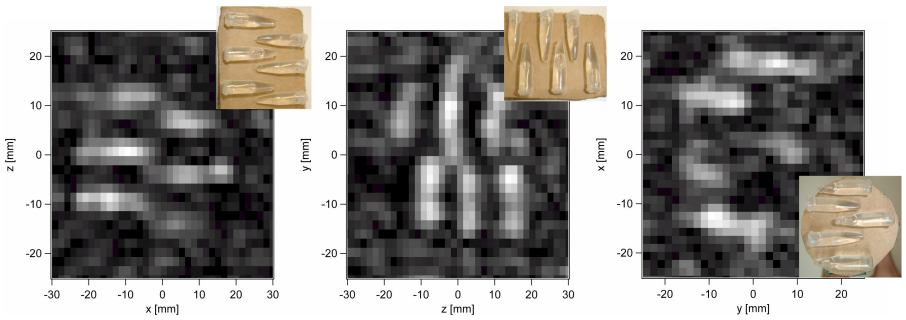

Figure 14: Magnetic resonance images of an arrangement of small sample tubes to show the distortion in the gradient fields. The insets show photographs of the actual sample arrangements.

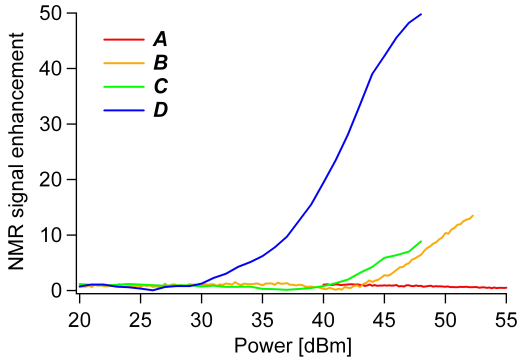

Figure 15: With the right timing, the effect of DNP can be observed. Only a slight depolarization at high power can be measured (A). The performance can be improved by reducing the number of connectors and attaching the coaxial cable directly to the ESR resonator. The depolarization is observed at lower power levels (zero polarization at $\sim 41\,\mathrm{dBm}$) and an enhancement of up to ~ 10 at $\sim 50\,\mathrm{dBm}$ ($= 100\,\mathrm{W}$) is visible (B). By adding a low-pass filter on the ESR signal the effect of DNP can be measured at slightly lower power levels (C). A significant step to much lower power levels is achieved by finding the right g-factor of the free radical. Zero polarization occurs already at $\sim 26\,\mathrm{dBm}$ ($\approx 0.4\,\mathrm{W}$) and an enhancement of ~ 50 is observed at $\sim 47\,\mathrm{dBm}$ ($\approx 50.1\,\mathrm{W}$) (D). The effect of depolarization before an enhancement can be seen in each measurement and is prove for the principle of negative enhancement described in Section 2.3.1.

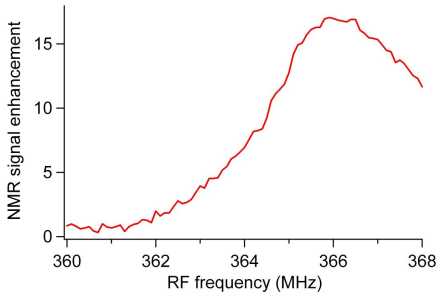

Figure 16: Dynamic nuclear polarization at different ESR frequencies at a constant magnetic field shows the effect of changing the free electron's g-factor. Being off too far from the actual g-factor can lead to no enhancement in the NMR signal.

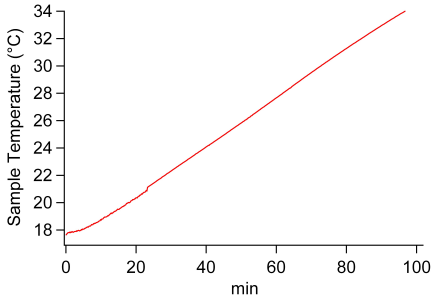

Figure 17: The sample temperature increases significantly during an experiment with an ESR pulse of 2 seconds every 10 seconds over 100 minutes.

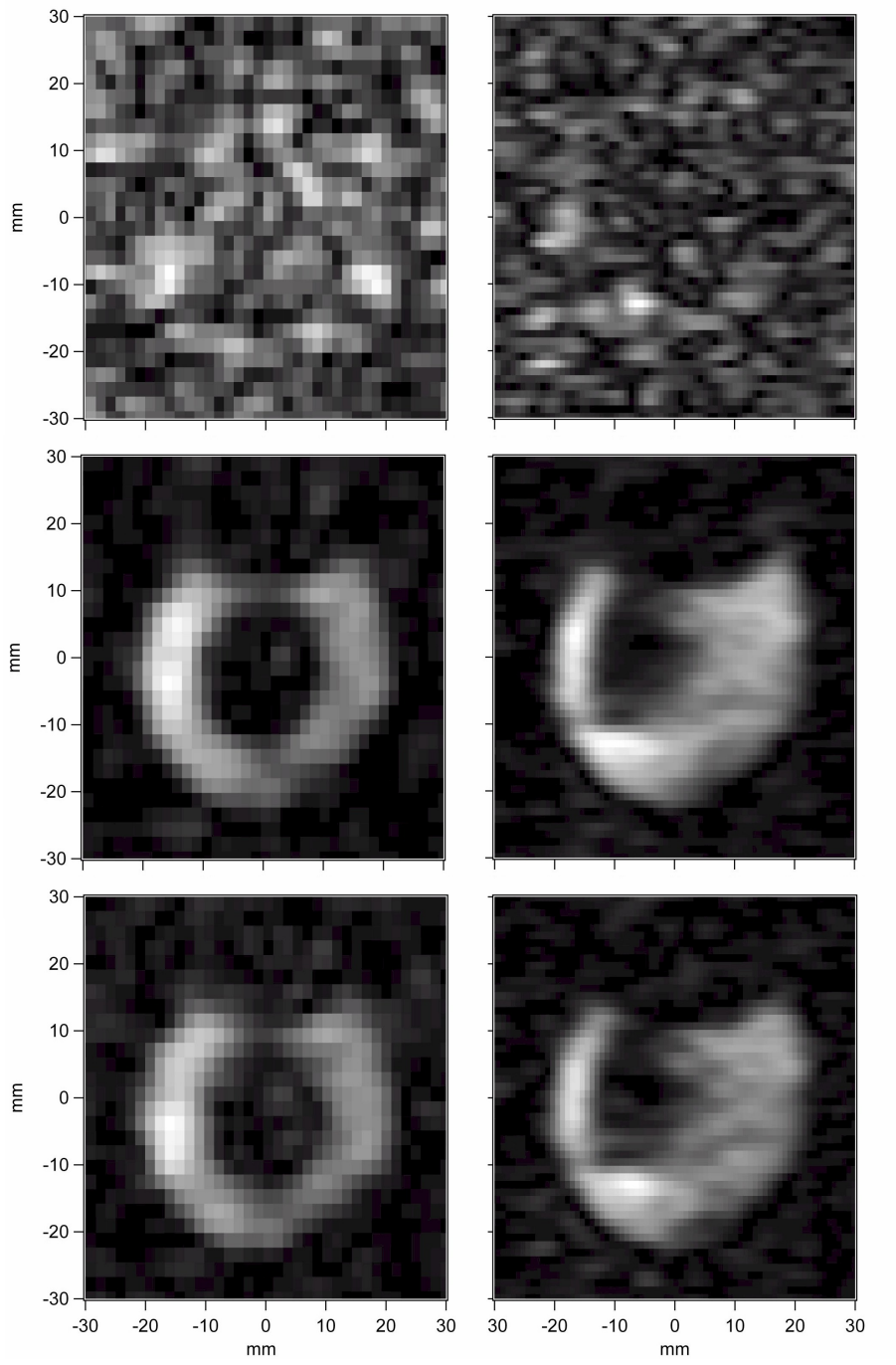

Figure 18: The two series of projection images show magnetic resonance images of non-hyperpolarized material (top row), the same image with hyperpolarized material (middle row), and the difference between the two images (bottom row). All images are single acquisitions (no averaging) at a magnetic field of 11.6 mT. The power of the ESR pulse in the left and the right series are 20 W and 40 W, respectively, resulting in a signal enhancement of about 15 and 20, respectively.

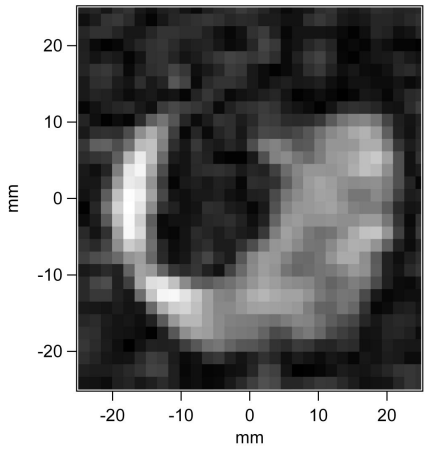

Figure 19: Slice selected image of a sample containing hyperpolarized material. The slice thickness is 1 cm. The image is taken at a magnetic field of 11.8 mT. The power of the ESR pulse is 40 W resulting in a signal enhancement of about 20. The image is averaged over 10 acquisitions only.

SECTION 5

Conclusion and Outlook

5.1 A Working System

A magnetic resonance imaging system was designed and built. It was proven to be capable of imaging, performing dynamic nuclear polarization and Overhauser-enhanced imaging at low magnetic fields of 10 - 20 mT.

Field-cycling allows the use of even lower magnetic field strengths in order to reduce the ESR irradiation frequency and hence lower the absorbed power. In field-cycling the magnetic field strength B_0 is switched between two levels during the pulse sequence. The field is reduced for the ESR irradiation and is ramped up for the NMR pulses, imaging gradients and signal detection [34]. This method was developed to counter the problem of poor image quality at very low magnetic fields [35].

The implementation of field-cycling could also help in this setup to improve image quality significantly. The feasibility of this method in the present setup has to be carefully checked first, especially the limits of the electromagnet and magnet power supply. The maximal current that can be applied plays a role as well as the time it takes to ramp between the two magnetic fields.

5.2 Upcoming Experiments

There are a lot of experiments to be performed to take steps towards *in vivo* applications. Silicon nanoparticles and perfluorocarbon emulsion particles both show great potential as targeted MRI contrast agents and as trackable drug delivery agents.

5.2.1 Silicon Nanoparticles

^{29}Si has a nuclear spin of 1/2, but a NMR signal could not be measured in the present setup. The natural abundance of less than 5 % [36] and the gyromagnetic ratio lowered by a factor of more than 5 compared to the proton [37] decrease the measurable signal by a significant amount compared to water, so that a detection at low fields was not possible.

However, DNP on silicon nanoparticles has been performed using free electrons of defects between the bulk silicon and a silicon oxide layer [18, 19]. Imaging hyperpolarized Si nanoparticles might be possible even at low fields. The implementation of field-cycling would surely be of interest for this purpose and could ease measuring ^{29}Si.

Biofunctionalization of nanoparticle surfaces [18] could allow not only targeting but also provide an alternative approach to perform magnetic resonance on the particle. Proton containing molecules attached to a particle's surface could possibly be dynamically hyperpolarized via the same defects. This would give a more easily measurable NMR signal from protons. It has to be clarified first if the spatial distribution of the free electron's wave function actually allows the electron-nuclear interactions necessary for DNP. The thickness of the oxide and thus the distance of the attached molecules to the defects will play an

important role and needs to be controllable in a reliable manner to customize the particles optimally.

To overcome these limitations to a certain extent, ^{13}C enriched molecules could be used for the surface functionalization. It could possibly transfer a nuclear spin polarization to attached protons due to its spin 1/2. The amount of this transfer also has to be estimated first.

Silicon nanoparticles are interesting for *in vivo* applications because they could possibly replace mostly toxic free radicals. Biocompatibility [38], biodegradability [39] and *in vivo* studies [40] of porous silicon revealed no evidence of toxicity. MRI of hyperpolarized ^{29}Si would be interesting since it's not naturally occurring in the body and could therefore provide very high image contrast with no background signal.

5.2.2 Perfluorocarbon Nanoparticles

NMR of ^{19}F has several advantages compared to ^{29}Si. Its nuclear moment is about 0.94 times the one of a proton [37] and its natural abundance is nearly 100 % [41], giving a NMR signal nearly as strong as the proton NMR signal. ^{19}F also isn't naturally occurring in the body, could provide high image contrast with basically no background signal and is therefore interesting for MRI.

Liquid perfluorocarbon (PFC)-based nanoparticles are composed with an outer phospholipid monolayer with a nominal diameter of ~ 250 nm. These PFC emulsion nanoparticles are 98 % PFC by volume and the C-F bond is chemically and thermally stable and essentially biologically inert [42]. No toxicity or carcinogenicity effects have been reported [43]. PFC nanoparticles may be functionalized for targeted magnetic resonance imaging and to effectively deliver therapeutic agents to target sites by incorporation of homing ligands into the lipid monolayer [44, 45].

The limited concentration of fluorine when PFC nanoparticles are in solution makes it difficult to achieve a detectable overall concentration [42]. Dynamic nuclear polarization of fluorocarbons has been reported [46, 47] and helps detecting a signal of very low fluorine concentrations.

Preliminary magnetic resonance measurements of a perfluorocarbon (Perfluorooctyl bromide 99 %, Sigma-Aldrich, St. Louis, MO) have already been performed in the present setup. Hyperpolarizing a perfluorocarbon compound with a free radical would be the next step. Thereafter, finding ways of DNP in emulsion particles without a free radical could be essential for future *in vivo* applications.

Acknowledgments

First of all, I'd like to thank physics undergraduate Winston Yan. His catching inquisitiveness and enthusiasm about science made it a pleasure to work with him and to learn a lot of new things. His work in the lab was always very helpful. Many thanks also go to Maja Cassidy for her helping hands and mind to solve problems, for her patience to answer questions and for animated discussions. She has always been a reliable source of solutions and new ideas. I'd also like to thank Menyoung Lee for his thoughts and help on many problems throughout the project.

My thanks also go to my predecessors, Alex Johnson, Jacob Aptekar, and Alex Ogier, who had done a lot of work on the setup and programmed many procedures to make my work much easier. Further thanks go to Ross Mair and Matthew Rosen for their advice and helpful discussions.

Additionally, I'd like to thank all other group members of the Marcus Lab, mostly Ferdinand Kuemmeth, Christian Barthel, Jimmy Williams, Max Lemme. They've always been around when needed to answer questions, give a helping hand and help out with strong arms. Thanks go to the whole group for all the scientific and non-scientific support throughout my project at Harvard. I enjoyed my time with all of you.

Many thanks go to Prof. Charles Marcus and Prof. Dominik Zumbühl who gave me the opportunity to pursue my master's thesis in an excellent lab at Harvard University. It gave me the possibility to work in a new environment and meet many interesting people. Their support was always a great motivation.

I'd also like to thank the Swiss Nanoscience Institute (SNI) for making this work possible with a traveling grant.

Last but not least, I'd like to thank my family who supported me not only during the master's thesis but throughout my whole studies. It all wouldn't have been possible with their great help.

References

[1] I. I. Rabi, J. R. Zacharias, S. Millman, P. Kusch, *Physical Review* **53**, 318 (1938).

[2] F. Bloch, W. W. Hansen, H. E. Packard, *Physical Review* **69**, 127 (1946).

[3] E. H. Purcell, H. C. Torrey, R. V. Pound, *Physical Review* **69**, 37 (1946).

[4] Http://en.wikipedia.org/wiki/NMR. Last viewed 06/12/2009.

[5] P. C. Lauterbur, *Nature* **242**, 190 (1973).

[6] S. Subramanian, K.-I. Matsumoto, J. B. Mitchell, M. C. Krishna, *NMR in Biomedicine* **17**, 263 (2004).

[7] N. Blow, *Nature* **458**, 925 (2009).

[8] Http://en.wikipedia.org/wiki/Dynamic_Nuclear_Polarisation. Last viewed 06/12/2009.

[9] D. J. Lurie, *In Vivo EPR (ESR): Theory and Application* (Kluwer Academic, 2001).

[10] A. W. Overhauser, *Physical Review* **92**, 411 (1953).

[11] T. R. Carver, C. P. Slichter, *Physical Review* **102**, 975 (1956).

[12] D. J. Lurie, *The British Journal of Radiology* **74**, 782 (2001).

[13] M. E. Akerman, W. C. W. Chan, P. Laakkonen, S. N. Bhatia, E. Ruoslahti, *Proceedings of the National Academy of Sciences* **99**, 12617 (2002).

[14] R. Weissleder, K. Kelly, E. Y. Sun, T. Shtatland, L. Josephson, *Nature Biotechnology* **23**, 1418 (2005).

[15] D. Simberg, *et al.*, *Proceedings of the National Academy of Sciences* **104**, 932 (2007).

[16] M. Suchanek, *et al.*, *Acta Physica Polonica A* **107**, 491 (2005).

[17] J. C. Leawoods, D. A. Yablonskiy, B. Saam, D. S. Gierda, M. S. Conradi, *Concepts in Magnetic Resonance* **13**, 277 (2001).

[18] J. W. Aptekar, *et al.*. ArXiv:0902.0269v1.

[19] A. E. Dementyev, D. G. Cory, C. Ramanathan, *Physical Review Letters* **100**, 127601 (2008).

[20] M. T. Vlaardingerbroek, J. A. den Boer, *Magnetic Resonance Imaging: Theory and Practice* (Springer, 1999), second edn.

[21] Http://en.wikipedia.org/wiki/Relaxation_(NMR). Last viewed 06/12/2009.

[22] Http://www.cis.rit.edu/htbooks/nmr/. Last viewed 06/12/2009.

[23] Http://www.cis.rit.edu/htbooks/mri/. Last viewed 06/12/2009.

[24] D. I. Hoult, R. E. Richards, *Journal of Magnetic Resonance* **24**, 71 (1976).

[25] L. E. Crooks, *et al.*, *Radiology* **151**, 127 (1984).

[26] E. M. Haacke, R. W. Brown, M. R. Thompson, R. Venkatesan, *Magnetic Resonance Imaging: Physical Principles and Sequence Design* (Wiley-Liss, 1999), third edn.

[27] B. D. Armstrong, S. Han, *The Journal of Chemical Physics* **127**, 104508 (2007).

[28] D. Grucker, *et al.*, *Journal of Magnetic Resonance, Series B* **106**, 101 (1995).

[29] J. H. Ardenkjaer-Larsen, *et al.*, *Journal of Magnetic Resonance* **133**, 1 (1998).

[30] B. A. Chronik, Optimization of gradient coil technology for human magnetic resonance imaging, Ph.D. thesis, University of Western Ontario (2000).

[31] D. W. Alderman, D. M. Grant, *Journal of Magnetic Resonance* **36**, 447 (1979).

[32] Http://www.realhamradio.com/DC_54_mhz_lowpass_filter.htm. Last viewed 06/02/2009.

[33] Http://www.e-mri.org/. Last viewed 06/12/2009.

[34] D. J. Lurie, K. Mäder, *Advanced Drug Delivery Reviews* **57**, 1171 (2005).

[35] D. J. Lurie, *et al.*, *Journal of Magnetic Resonance* **84**, 431 (1989).

[36] Http://en.wikipedia.org/wiki/Isotopes_of_silicon. Last viewed 06/12/2009.

[37] Http://www18.wolframalpha.com/input/?i=29Si+1H+19F+magnetic+moment. Last viewed 06/12/2009.

[38] S. C. Bayliss, R. Heald, D. I. Fletcher, L. D. Buckberry, *Advanced Materials* **11**, 318 (1999).

[39] L. T. Canham, *Advanced Materials* **7**, 1033 (1995).

[40] J.-H. Park, *et al.*, *Nature Materials* **8**, 331 (2009).

[41] Http://en.wikipedia.org/wiki/Isotopes_of_Fluorine. Last viewed 06/12/2009.

[42] G. M. Lanza, *et al.*, *Current Topics in Developmental Biology* **70**, 57 (2005).

[43] M. P. Krafft, *Advanced Drug Delivery Reviews* **47**, 209 (2001).

[44] N. R. Soman, G. M. Lanza, J. M. Heuser, P. H. Schlesinger, S. A. Wickline, *Nano Letters* **8**, 1131 (2008).

[45] N. R. Soman, J. N. Marsh, G. M. Lanza, S. A. Wickline, *Nanotechnology* **19**, 185102 (2008).

[46] A. Modica, D. J. Lurie, M. Alecci, *Physics in Medicine and Biology* **51**, N39 (2006).

[47] M. Chapellier, L. Sniadower, G. Dreyfus, H. Alloul, J. Cowen, *Journal de Physique* **45**, 1033 (1984).

SECTION A

Appendix

A.1 Electromagnet Field Characterization

The calibration of the magnetic field (Fig. 20) at the center of the electromagnet was performed by the manufacturer GMW.

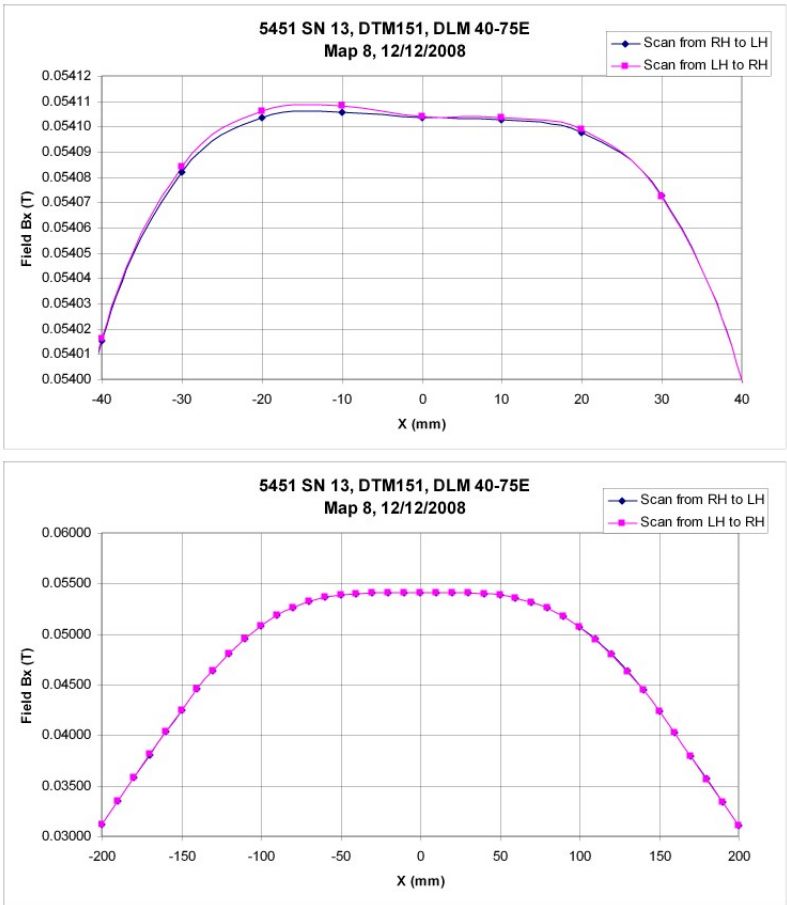

Figure 20: Scans of the magnetic field along the magnet's axis.

A.2 NMR Coil Design

A schematic of the NMR coil circuit is shown in Fig. 21.

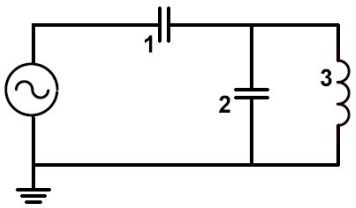

Figure 21: Design of the NMR coil circuit. Capacitors *1* and *2* both consist of a permanent chip capacitor and a variable capacitor. Capacitance *1* is used to match the coil's impedance to 50 Ω, capacitance *2* is needed to tune the circuit's resonance frequency. *3* is the saddle coil.

A.3 ESR Coil Design

The schematic used to design the ESR resonator is derived in Fig. 22

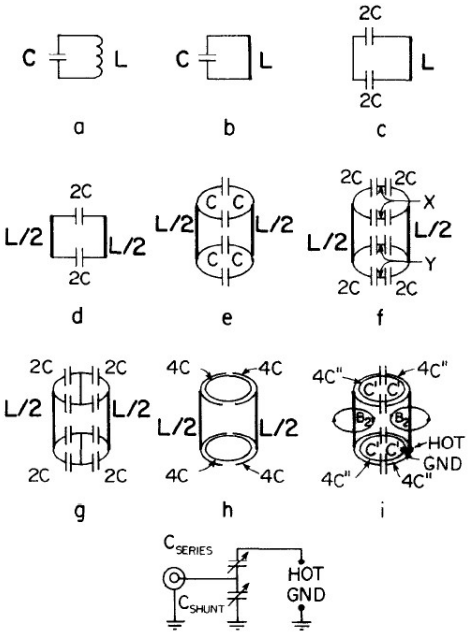

Figure 22: The schematic of the Alderman-Grant resonator derived from a simple LC circuit [31]. In the original design, chip capacitors were used for the capacitance C' whereas in the present imager setup those capacitors have been left out and C' is only formed by the copper sheets being close to each other.

A.4 High Power Low-Pass Filter Design

A schematic (Fig. 23) and a picture (Fig. 24) of the high power low-pass filter for the ESR coil with a cutoff frequency of about 400 MHz are shown. The measured transmission of the filter is shown in Fig. 25.

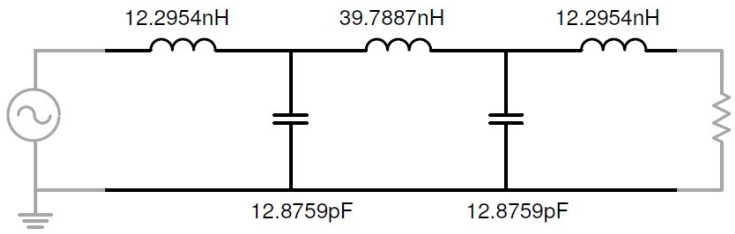

Figure 23: The schematic and calculated values for the low-pass filter with 5 stages and inductor input to have a cutoff frequency of 400 MHz.

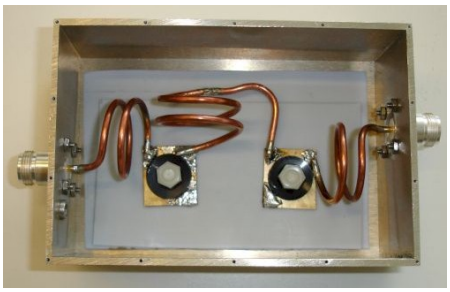

Figure 24: Picture of the high power low-pass filter.

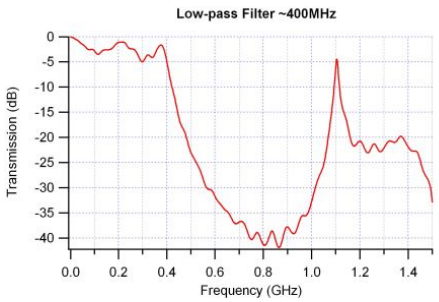

Figure 25: Transmission of the low-pass filter.

SECTION B

Useful Numbers

Table 1 shows some general parameters that are often used during the experiments.

Table 1: Some parameters used for the experiments

Nuclei:	$\gamma_H = 42.577 \frac{MHz}{T}$	$\gamma_F = 40.017 \frac{MHz}{T}$	$\gamma_{Si} = 8.435 \frac{MHz}{T}$
Electrons:	$\gamma_{TEMPO} = 28.820 \frac{GHz}{T}$	$\gamma_e = 28.025 \frac{GHz}{T}$	
	$g_{TEMPO} = 2.0591$	$g_e = 2.0023$	
Magnet:	$0.7732 \frac{mT}{A}$	$70 \cdot 10^{-6} \frac{A}{ppm}$	
Gradients:	$G_x = 18.454 \frac{mT}{m}$	$G_y = 13.420 \frac{mT}{m}$	$G_z = 15.658 \frac{mT}{m}$
	@ Peavey single channel, full power (2000 W), per V input		
sinc-pulse:	$\tau_0 = \frac{1}{\Delta f}$	$\Delta f = \gamma \cdot \Delta z \cdot G_z$	$t_{90} = n_0 \cdot \tau_0$ $(n_0 \geq 4)$
TEMPO:	$M_W = 156.25 \frac{g}{mol}$		